Structural engineering of nanoporous anodic aluminium oxide by pulse anodization of aluminium

WOO LEE*†, KATHRIN SCHWIRN, MARTIN STEINHART, ECKHARD PIPPEL, ROLAND SCHOLZ AND ULRICH GÖSELE

Max Planck Institute of Microstructure Physics, Weinberg 2, D-06120 Halle, Germany
†Present address: Korea Research Institute of Standards and Science (KRISS), Taejon 305-600, Korea
*e-mail: woolee@kriss.re.kr

Published online: 23 March 2008; doi:10.1038/nnano.2008.54

Nanoporous anodic aluminium oxide has traditionally been made in one of two ways: mild anodization or hard anodization. The first method produces self-ordered pore structures, but it is slow and only works for a narrow range of processing conditions; the second method, which is widely used in the aluminium industry, is faster, but it produces films with disordered pore structures. Here we report a novel approach termed "pulse anodization" that combines the advantages of the mild and hard anodization processes. By designing the pulse sequences it is possible to control both the composition and pore structure of the anodic aluminium oxide films while maintaining high throughput. We use pulse anodization to delaminate a single as-prepared anodic film into a stack of well-defined nanoporous alumina membrane sheets, and also to fabricate novel three-dimensional nanostructures.

Nanoporous anodic aluminium oxide (AAO) with self-organized hexagonal arrays of uniform parallel nanopores has been used for various applications in the fields of sensing, storage, separation, and the synthesis of one-dimensional nanostructures[1–3]. Previously, self-ordered AAOs have been obtained by mild anodization (MA) within limited processing windows (that is, self-ordering regimes)[4–7]. The accessible pore diameters (D_p) and interpore distances (D_{int}) are limited by the self-ordering requirement. However, MA is slow, and it takes more than two days of processing time to obtain nanoporous AAOs that are suitable for applications, so hard anodization (HA) of aluminium, a faster process that was invented in the early 1960s[8,9], is an attractive alternative. Classical HA is carried out at relatively low temperatures and high current densities ($j > 50$ mA cm^{-2}) by using sulphuric acid (H_2SO_4), and has routinely been used in the aluminium industry to produce anodic films of high technical quality at an efficient rate of production (typically, 50–100 μm h^{-1}). However, the pores of the resulting anodic films are less ordered than those produced by MA processes. This has prevented the direct implementation of classical HA processes into current nanotechnology research.

Recently, the fabrication of self-ordered AAO was demonstrated under high anodization potentials and current densities (up to 70 V and 200 mA cm^{-2}, respectively) using an aged sulphuric acid solution[10], far outside the MA regime (H_2SO_4: 25 V and 2–4 mA cm^{-2}) but similar to the anodization conditions for HA. Unfortunately, the resulting AAOs were mechanically unstable, with a strong tendency towards crack development under the influence of even weak mechanical forces. More recently our group developed an $H_2C_2O_4$-based HA, which enabled between 25 and 30 times faster growth (compared to MA) of long-range ordered and mechanically robust AAOs in a self-ordering regime characterized by $D_{int} = 200–300$ nm (ref. 11). It was found that the current density (that is, the electric field strength E at the pore bottom) is an important parameter governing not only the structural parameters of AAO (D_{int}, porosity and thickness of the barrier layer), but also the self-organization of the oxide nanopores for a given anodization potential U_{HA} (refs 11–13). Based on these observations, the fabrication of novel AAO membranes with periodically modulated diameters of nanopores was realized, demonstrating that the combination of conventional MA and the newly developed HA could offer a new degree of freedom for tailoring the pore structure of AAOs by combining properties from the two anodization processes[11]. However, each modulation step required the exchange of the electrolyte solutions in order to satisfy both MA and HA processing conditions[11].

Here, we report a novel approach for continuous structural engineering of nanoporous AAO based on pulse anodization of aluminium under a potentiostatic condition using H_2SO_4. Periodic pulses consisting of a low-potential pulse followed by a high-potential pulse were applied to achieve MA and HA conditions, respectively. We show that combining MA and HA conditions by deliberately designing the pulse sequences allows tailoring of the pore structure as well as the chemical composition of the resulting AAO along the pore axes. This enabled us not only to completely delaminate a single as-prepared anodic film into a stack of well-defined AAO membrane sheets, but also to realize novel three-dimensional (3D) porous architectures that have the potential to be useful for a broad range of nanotechnology applications.

PULSE ANODIZATION OF ALUMINIUM

Recent studies have showed that D_{int} of AAO formed under conventional MA conditions using H_2SO_4, $H_2C_2O_4$ and H_3PO_4 is

linearly dependent on the applied voltage U_{MA}, with a proportionality constant $\zeta_{MA} = 2.5$ nm V^{-1} (refs 14–16). The proportionality constant $\zeta_{HA} = 1.8–2.0$ nm V^{-1} for AAO films formed by the HA processes turned out to be lower than for the MA processes[10–13,17]. For HA at a given potential U_{HA}, the current density j decreases exponentially as a function of time after an initial sharp surge, unlike in conventional MA processes where the current density is maintained at a steady-state value throughout the anodization[11–13]. D_{int} (or cell size) increases with decreasing current density for a given HA potential U_{HA} (refs 11–13). Based on these experimental findings, we suggested that the current density needs to be maintained at a certain level to obtain long-range ordered anodic alumina with a desired D_{int} for HA at a given potential U_{HA} (ref. 11). In a pulse anodization combining both MA and HA, therefore, these points have to be carefully taken into consideration when choosing pulse parameters (U_{HA} and pulse duration τ_{HA}) in order to match the D_{int} of HA-AAO to that of MA-AAO (D_{int}-matching). Otherwise, disordering or branching of pores will occur[18].

Figure 1 shows a current–time transient during pulse anodization of aluminium. A typical pulse profile is schematically illustrated in Fig. 1a. The pulses consist of an MA pulse ($U_{MA} = 25$ V and $\tau_{MA} = 180$ s) followed by an HA pulse ($U_{HA} = 35$ V and $\tau_{HA} = 0.1$ s). As shown in Fig. 1b, a typical recovery effect was observed for MA pulses, similar to other conventional MA processes, where current flow is large at the initial stage, hits a minimum value, and increases gradually to reach a steady value after passing through a current overshoot[18–20]. However, on applying an HA pulse the current increases steeply for a short period of time and then decreases exponentially.

Note that we could not achieve continuous pulse anodization of aluminium by using oxalic acid (0.3 M $H_2C_2O_4$, 1 °C) due to delayed current recovery during MA pulses under a similar electrochemical condition to H_2SO_4 anodization. In contrast to the case of H_2SO_4-based pulse anodization, current recovery was not observed within a reasonable period of time when we applied an MA pulse ($U_{MA} = 40$ V) immediately after a short high-potential pulse ($U = 53$ V, $\tau = 0.1$ s) (see Supplementary Information, Fig. S1). This is probably due to the formation of a thick, dense barrier oxide upon pulsing with a high anodization potential ($U = 53$ V). We interpret these observations to indicate that the barrier oxide formed by the high-potential pulse (the HA pulse) in H_2SO_4-based anodization is not compact enough to prevent the passage of ions under the subsequent low-potential pulse (the MA pulse). However, if the experiments were conducted at room temperature (18 °C) and not at 1 °C, the recovery effect could be observed, and thus continuous $H_2C_2O_4$-based pulsed anodization was accomplished under these conditions (see Supplementary Information, Figs S2–S5).

A representative scanning electron microscopy (SEM) image of AAO formed by pulse anodization is shown in Fig. 2a. Pores were widened by immersing the as-prepared AAO in 5 wt% H_3PO_4 (45 °C) before SEM investigation in order to help in the visualization of pores. Parallel alignment of pores normal to the surface of the membrane is evident from the micrograph. As indicated by white arrowheads, a series of horizontal lines with a periodic spacing (~231 nm) can clearly be seen. The spacing between lines corresponds to the thickness of the MA-AAO slabs.

FRACTURE MODES OF AAOs

In pulse anodization, pulse durations (τ_{HA} and τ_{MA}) determine the thicknesses of anodized segments at given anodization potentials (U_{HA} and U_{MA}). Figure 2b,c shows cross-sectional SEM images of AAO formed by applying a series of potential pulses, comprising

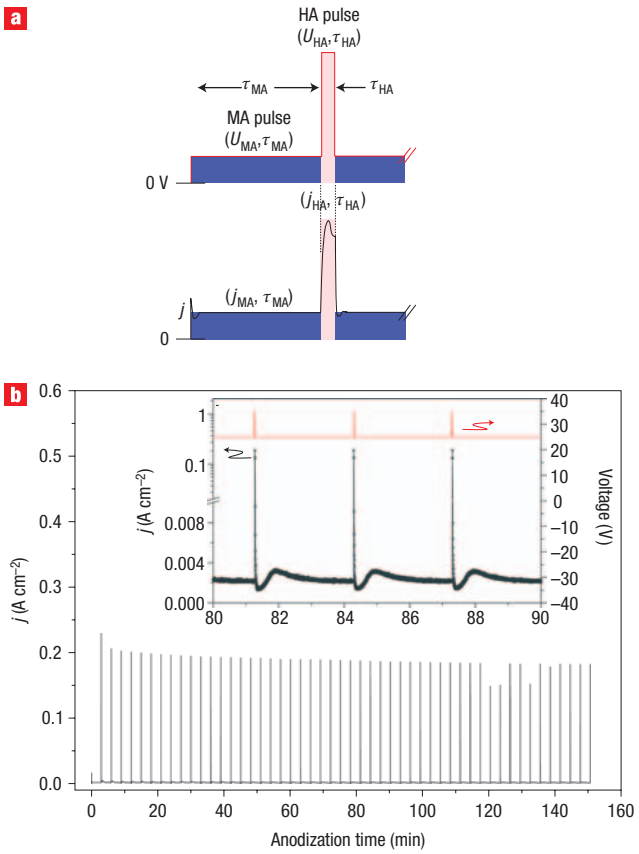

Figure 1 Pulse anodization. **a**, Pulse scheme used for pulse anodization of aluminium, where U_{MA} and U_{HA} denote the anodization potentials used to achieve MA and HA conditions, respectively, and τ_{MA} and τ_{HA} denote pulse durations for the respective anodizations (top: an applied potential pulse profile; bottom: a current profile). **b**, A typical current–time (j–t) transient during pulse anodization of aluminium. Pulses consisting of an MA pulse (U_{MA}=25 V and τ_{MA}=180 s) followed by an HA pulse (U_{HA}=35 V and τ_{HA}=0.1 s) were applied. Inset: an enlarged j–t curve at t=80–90 min.

an MA pulse with $U_{MA} = 25$ V and $\tau_{MA} = 120$ s followed by an HA pulse with $U_{HA} = 35$ V and $\tau_{HA} = 0.5$ s. It is clear that an increase in τ_{HA} results in thicker HA-AAO slabs when compared with the sample shown in Fig. 2a. It is worth mentioning that MA- and HA-AAOs exhibit different fracture modes along the vertical direction of AAO against external stresses, as is evident from Fig. 2b,c. For MA-AAO slabs, cracks propagated through the centre of pores from pore to pore (that is, the cleavage plane A–A′ in Fig. 2d). For HA-AAO slabs, on the other hand, the fracture propagated along cell boundaries and not through the centre of the pores (that is, the cleavage plane B–B′ in Fig. 2d). Cleavage through the cell boundaries in AAO formed under H_2SO_4-HA resulted even in single Al_2O_3 nanotubes or bundles of tubes (so-called "Keller-Hunter-Robinson cells"[21])[15], as indicated by the white arrowheads in Fig. 2c. The different fracture behaviours of H_2SO_4-AAOs formed under HA and MA conditions were discussed two decades ago[21,22], pointing out that the fracture behaviour affects the mechanical properties (for example, wear resistance) of anodic films. Recently, it was suggested that the weak junction strength of cells in AAOs formed by high-field anodization (that is, HA-AAOs) is responsible for preferred cleavage along the cell boundaries[10].

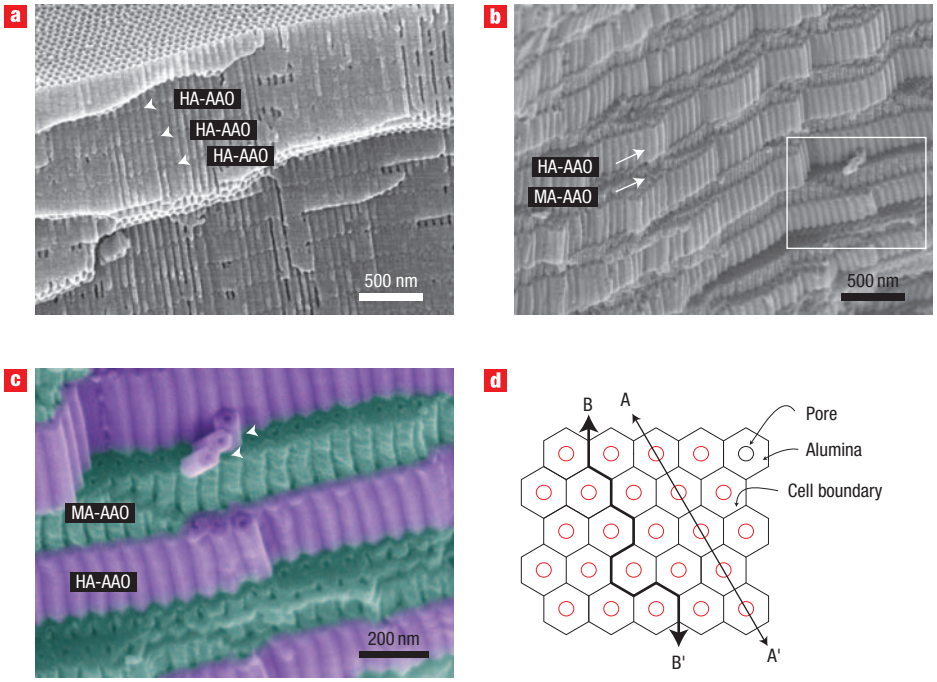

Figure 2 Anodic aluminium oxide. **a**, A representative SEM image of AAO prepared by pulse anodization (U_{MA}=25 V, τ_{MA}=120 s, U_{HA}=35 V and τ_{HA}=0.1 s). Pores were widened by using 5 wt% H_3PO_4 (45 °C) before SEM investigation in order to assist visualization of the pores. **b**, Cross-sectional SEM image of AAO formed by pulse anodization (U_{MA}=25 V, τ_{MA}=120 s, U_{HA}=35 V, τ_{HA}=0.5 s). **c**, Magnified view of the area marked with a white rectangle in **b**. The white arrowheads in **c** indicate alumina nanotubes (so-called "Keller-Hunter-Robinson cells"), which have separated from the HA-AAO slab. **d**, Schematic illustrating two different fracture modes: the A–A′ cleavage plane for MA-AAO and the B–B′ cleavage plane for HA-AAO.

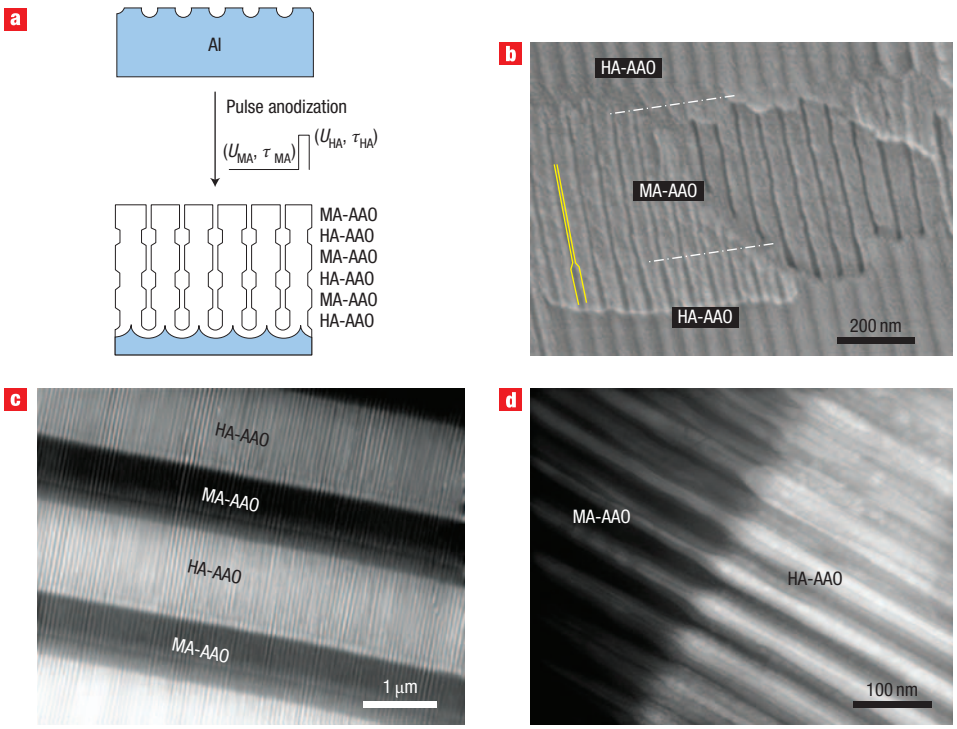

Figure 3 Modulation of pore diameter. **a**, Scheme for the fabrication of AAO with modulated pore diameters by pulse anodization. **b**, SEM image showing the cross-sectional view of an as-prepared AAO produced by H_2SO_4 pulse anodization (U_{MA}=25 V, τ_{MA}=180 s, U_{HA}=33 V, τ_{HA}=1 s). **c**,**d**, Cross-sectional TEM images of AAO formed by pulse anodization using 0.3 M H_2SO_4 (U_{MA}=25 V, τ_{MA}=180 s, U_{HA}=37 V, τ_{HA}=1 s), showing modulated pore diameter. Panel **c** shows a lower magnification image showing an overview and panel **d** a higher magnification image taken at the interface of the MA and HA-AAO slabs. Dark and bright image contrast areas correspond to MA- and HA-AAO segments, respectively.

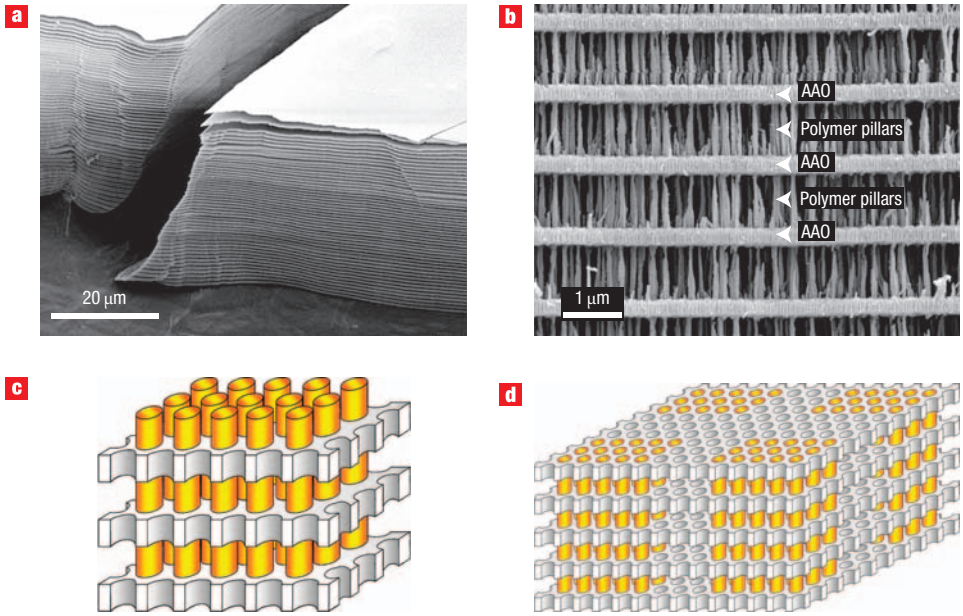

Figure 4 Delamination of AAO. **a**, SEM image of 3D stacks of MA-AAO slabs. The entire MA-AAO segment slabs were delaminated from an as-prepared AAO by selective removal of HA-AAO segments using 5 wt% H_3PO_4 (45 °C). **b**, SEM image of a polymer nanopillars/AAO composite microstructure, with the MA-AAO slabs supported by PS nanopillars. This micrograph was obtained from the edge of a specimen. **c**, Idealized structure of the composite microstructure. **d**, Schematic of the envisaged structure combining micro- and nanostructuring in which columns of a material are infiltrated only in areas defined by lithography.

In order to gain insight into the origin of the weak junction strength between cells in HA-AAO, we focused on characterizing the microstructures of samples prepared under MA and HA conditions. It has been well-established that sub-nanometre-sized cavities (or voids) that cannot be observed in focus because of $<5\%$ contrast in transmission electron microscopy (TEM) observation, can be visualized by viewing them out of focus by taking advantage of Fresnel diffraction effects, where a cavity appears to be a dark spot with a bright periphery under overfocus and a light spot with a dark periphery under underfocus[23,24]. TEM investigation on as-prepared HA-AAO disclosed the presence of voids along the cell boundaries as well as at the triple junctions where three cells meet, in contrast to the case of MA-AAO (see Supplementary Information, Fig. S6). In addition, it was found, from comparative TEM investigations on HA- and MA-AAO samples, that nanometre-sized cavities are present in the oxide matrix constituting the pore walls of HA-AAO (see Supplementary Information, Fig. S6). The distribution of cavities was found to be non-uniform, but localized mainly around the pores. This observation implies again that anodic oxide formed by HA is less compact than that prepared by the MA process.

Previously it was found that spherical voids, each of which contains a crystalline γ-Al_2O_3 particle, are present in porous AAO only at the triple junctions and that the size of the voids increases with anodization voltage[25,26]. It was proposed that cation (and/or metal) vacancy condensation is responsible for the formation of voids at the triple junctions of the barrier layer, where flux of cation vacancy is greatest due to the presence of a high degree of lattice disorder[27]. It was also suggested that the vacancy condensates coincide with protrusions of aluminium metal into the barrier layer, resulting in texturing of the aluminium substrate with a hexagonal cellular topography. However, this mechanism does not reasonably account for the presence of voids in the pore wall oxide as well as at the cell boundaries, although there was an attempt to explain the small voids at the cell boundaries based on this model[28].

The formation of voids along the cell boundaries and in the pore wall oxide could be related to the pronounced evolution of oxygen gas bubbles from the anode surface during HA of aluminium, which is mainly due to the oxidation of the O^{2-} ions of the anodic oxide at the metal/oxide interface (that is, $O^{2-} \rightarrow 1/2O_2 + 2e^-$)[29,30]. Recently, it was suggested that field-induced plastic flow of oxide material from the centre of the pore base toward the cell boundary may result in accumulation of mechanical stress along the cell boundaries in the form of compressive stress between neighbouring cells[31,32], which is a driving force for two-dimensional (2D) hexagonal ordering of cells[33]. This dynamic mass transfer process could play a role in the formation of voids. We assume that a major fraction of oxygen gas is liberated from the bottom of pores to the surface of the anodic film through the pores after being nucleated and grown to increase their volume. The remaining fraction of oxygen gas bubbles may coalesce at the cell boundaries. Accordingly, the formation of voids along the cell boundaries during HA might be the origin of the weak junction strength of the cells, leading to cracking of AAO along the cell boundaries. A detailed discussion of the cracking behaviour of HA-AAO will be provided elsewhere.

STRUCTURAL AND COMPOSITIONAL MODULATIONS OF AAO

A very attractive structural feature of AAO prepared by pulse anodization is the presence of modulations of the pore diameters along the pore axes as shown in Fig. 3. Recently, we found from $H_2C_2O_4$-based HA that the porosity of HA-AAOs is about 30% lower than that of MA-AAOs[11]. As the pore diameter D_p is strongly affected by the dissolution velocity of alumina, which is determined by the pH value at the pore bottom[34], the reduced porosity could be attributed to enhanced proton activity at the bottom of the pores,

where significant Joule heating occurs as a result of the high current density (that is, high electric field E). On the other hand, the porosity of AAOs formed by H_2SO_4-HA turned out to be higher than that of AAOs formed by H_2SO_4-MA (Fig. 3), which is in agreement with recent results[10]. The observed opposite evolution of the porosity can be explained by considering the chemical composition of AAOs. The samples formed under H_2SO_4-HA conditions showed a higher level of impurities and less dense pore walls compared with MA samples. According to TEM-EDXS (energy dispersive x-ray spectroscopy) analysis performed on pulse-anodized samples, the amount of anionic impurities (mostly SO_4^{2-}) in HA-AAO turned out to be about 88% higher than in MA-AAO (see Supplementary Information, Table S1). Local chemical dissolution of the pore walls by the acid electrolyte during HA is expected to be much more significant for impure AAO formed by HA than for relatively pure AAO formed by MA, leading to an increase in porosity for H_2SO_4-HA as compared to their MA counterparts.

The high content of anionic impurities in AAO formed by HA pulses could be explained by high-field conduction theory, where the current density j is related to the voltage drop V across the barrier layer[35–37]:

$$j = \mathrm{A}\ \exp(\beta V/d), \qquad (1)$$

where A and β are material-dependent constants at a given temperature, and V/d is the effective electric field across the barrier layer with thickness d. It is known that as-prepared AAO is amorphous, and contains anionic impurities from the electrolyte used[37,38]. The amount of anionic impurities incorporated into AAO depends sensitively on the nature of the electrolyte and the anodization conditions. The pore walls of nanoporous AAO consist of two main layers: an inner layer of relatively pure oxide and an outer layer of anion-incorporated oxide. In our experiments the current density for an HA pulse was about two orders of magnitude higher than that for an MA pulse (see Fig. 1b). For a given thickness of the barrier layer the current density is related to the passage of ions through the barrier layer, so it is expected that the relative thickness of the pure, inner alumina layer of AAOs formed by HA pulses is smaller than that of AAOs formed by MA pulses, leading to a larger voltage drop across the barrier layer. Accordingly, the observed high current density for HA pulses can be associated with a high impurity content in AAO. Therefore, one can achieve a periodic compositional modulation in AAO by using H_2SO_4-based pulse anodization of aluminium, applying MA and HA sequentially.

As mentioned above, the higher impurity content and less dense pore walls in HA-AAO results in a poor chemical stability against etchants (for example, 5 wt% H_3PO_4). Thus, a periodic compositional modulation in AAO gives rise to an enhanced etching contrast between MA- and HA-AAOs, enabling the fabrication of AAO with a modulated pore structure, where the difference in the pore diameters of HA- and MA-AAO is much more pronounced than in as-prepared samples. In fact, we were even able to delaminate completely the entire MA-AAO segment slabs in the form of 2D sheets from an as-prepared AAO by selectively removing HA-AAO segments as shown in Fig. 4a. This process could provide a simple, continuous, and economic way for the mass production of nanoporous AAO sheets.

Our preliminary experimental results showed that novel 3D polymer nanopillar/AAO composite microstructures could be realized by taking advantage of the marked etching contrast between HA- and MA-AAO segments. Three-dimensional polymer nanopillar/AAO composite microstructures, in which MA-AAO slabs are supported by polymer pillars, were fabricated by pressure-driven melt-injection of polystyrene (PS) (molecular weight $\sim 1\times10^5$) into the nanopores of as-prepared AAO (ref. 39), followed by selective removal of HA-AAO segments using 5 wt% H_3PO_4 (45 °C) for 20 min. As shown in Fig. 4b, 2D MA-AAO slabs with an average thickness of 290 nm are supported by PS pillars. A schematic of the idealized structure is shown in Fig. 4c. In analogy to visible-light Bragg diffractors, the sample showed an interference effect due to the periodic modulation of the dielectric constants of the constituting materials (that is, Al_2O_3 and PS). It is expected that the present method can be readily extended to the realization of novel 3D photonic structures by combining it with previously established techniques for microstructuring of AAO as shown in Fig. 4d (ref. 40). Another intriguing perspective is the potential application of 3D polymer nanopillar/AAO composite microstructures as a material platform for phononic crystals or phononic/photonic hybrid crystals[41].

In summary, pulse anodizations of aluminium were conducted under potentiostatic conditions by using H_2SO_4. Pulses consisting of a low-potential pulse followed by a high-potential pulse were applied to achieve alternating MA and HA conditions. It was found that the effective electric field strength E impressed on the barrier oxide layer has profound implications on the anodic alumina formed by high-field anodization, determining not only the chemical stability but also the mechanical properties of anodic alumina. Structural engineering of nanoporous AAO along the film growth direction can be achieved by deliberately designing pulse sequences. It is expected that the present pulse anodization process combining both MA and HA can open up a new area in nanotechnology research and may also be applied for industrial processes.

METHODS

PULSE ANODIZATION

The aluminium substrate was electropolished using a 1:4 mixture solution of $HClO_4$ and CH_3CH_2OH. Surface-finished aluminium substrates were anodized under a regulated cell voltage of 25 V by using 0.3 M H_2SO_4 (1 °C) for 15 h. Afterwards, the resulting porous oxide layer was completely removed by immersing the resultant films in an acid mixture (1.8 wt% chromic acid and 6 wt% H_3PO_4) at 45 °C for 12 h. The resulting textured aluminium was used for pulse anodization. Pulse anodization was performed under potentiostatic conditions by applying a series of potential pulses comprising an MA pulse followed by an HA pulse. The anodized area of the aluminium substrate was 0.95 cm^2. After anodization, a free-standing AAO membrane was obtained by removing the underlying aluminium substrate with a solution containing 3.4 g $CuCl_2{\cdot}H_2O$, 100 ml 37 wt% HCl and 100 ml H_2O.

TEM INVESTIGATION

The microstructure of AAO membranes was investigated by TEM. The samples for cross-sectional and plane-view investigations were prepared by the following procedure. Membrane pieces were glued on silicon substrates with epoxy resin. After cutting the samples with a diamond wire, cross-sectional slices or planar membrane pieces were further thinned for electron transmission by standard methods (that is, mechanical polishing, dimpling and ion milling). TEM investigations were carried out using a conventional Philips CM20T microscope and EDX measurements in a Philips CM20FEG at 200 kV accelerating voltage.

Received 15 January 2008; accepted 15 February 2008; published 23 March 2008.

References

1. Martin, C. R. Nanomaterials—A membrane-based synthetic approach. *Science* **266,** 1961–1966 (1994).
2. Nicewarner-Peña, S. R. *et al.* Submicrometer metallic barcodes. *Science* **249,** 137–141 (2001).
3. Lee, S. B. *et al.* Antibody-based bio-nanotube membranes for enantiomeric drug separations. *Science* **296,** 2198–2200 (2002).
4. Masuda, H. & Fukuda, K. Ordered metal nanohole arrays made by a two-step replication of honeycomb structures of anodic alumina. *Science* **268,** 1466–1468 (1995).

5. Masuda, H., Hasegwa, F. & Ono, S. Self-ordering of cell arrangement of anodic porous alumina formed in sulfuric acid solution. *J. Electrochem. Soc.* **144,** L127–L130 (1997).
6. Li, A. P., Müller, F., Birner, A., Nielsch, K. & Gösele, U. Hexagonal pore arrays with a 50–420 nm interpore distance formed by self-organization in anodic alumina. *J. Appl. Phys.* **84,** 6023–6026 (1998).
7. Masuda, H., Yada, K. & Osaka, A. Self-ordering of cell configuration of anodic porous alumina with large-size pores in phosphoric acid solution. *Jpn. J. Appl. Phys.* **37,** L1340–L1342 (1998).
8. Csokán, P. & Sc, C. Ch. Hard anodizing: Studies of the relation between anodizing conditions and the growth and properties of hard anodic oxide coatings. *Electroplat. Metal Finishing* **15,** 75–82 (1962).
9. Lichtenberger-Bajza, E., Domony, A. & Csokán, P. Untersuchung der Struktur und anderer Eigenschaften von durch anodische Oxydation auf Aluminium erzeugten Hartoxydschichten. *Werkst. u. Korr.* **11,** 701–707 (1960).
10. Chu, S.-Z. *et al.* Fabrication of ideally ordered nanoporous alumina films and integrated alumina nanotubule arrays by high-field anodization. *Adv. Mater.* **17,** 2115–2119 (2005).
11. Lee, W., Ji, R., Gösele, U. & Nielsch, K. Fast fabrication of long-range ordered porous alumina membranes by hard anodization. *Nature Mater.* **5,** 741–747 (2006).
12. Lee, W., Nielsch, K. & Gösele, U. Self-ordering behavior of nanoporous anodic aluminium oxide (AAO) in malonic acid anodization. *Nanotechnology* **18,** 475713 (2007).
13. Schwirn, K. *et al.* Self-ordered anodic aluminum oxide (AAO) formed by H_2SO_4 hard anodization (HA). *ACS Nano* **2,** 302–310 (2008).
14. O'Sullivan, J. P. & Wood, G. C. Morphology and mechanism of formation of porous anodic films on aluminium. *Proc. R. Soc. Lond. A* **317,** 511–543 (1970).
15. Keller, F., Hunter, M. S. & Robinson, D. L. Structural features of oxide coatings on aluminum. *J. Electrochem. Soc.* **100,** 411–419 (1953).
16. Ebihara, K., Takahashi, H. & Nagayama, M. Structure and density of anodic oxide films formed on aluminium in oxalic acid solutions. *J. Met. Finish. Soc. Jpn* **34,** 548–554 (1983).
17. Li, Y., Zheng, M., Ma, L. & Shen, W. Fabrication of highly ordered nanoporous alumina films by stable high-field anodization. *Nanotechnology* **17,** 5105–5105 (2006).
18. Takahashi, H., Nagayama, M., Akahori, H. & Kitahara, A. Electron-microscopy of porous anodic oxide films on aluminum by ultra-thin sectioning technique. Part 1. The structural change of the film during the current recovery period. *J. Electron. Microscopy* **22,** 149–157 (1973).
19. Furneaux, R. C., Rigby, W. R. & Davidson, A. P. The formation of controlled-porosity membranes from anodically oxidized aluminum. *Nature* **337,** 147–149 (1989).
20. Murphy, J. F. & Michelson, C. E. *Anodizing Aluminum Proceedings* 83 (Aluminum Development Association, Nottingham, 1961).
21. Arrowsmith, D. J., Clifford, A. W. & Moth, D. A. Fracture of anodic oxide formed on aluminum in sulphuric acid. *J. Mater. Sci. Lett.* **5,** 921–922 (1986).
22. Wada, K., Shimohira, T., Amada, M. & Baba, N. Microstructure of porous anodic oxide films on aluminium. *J. Mater. Sci.* **21,** 3810–3816 (1986).
23. Rühle, M. R., Staiger, S., Katerbau, K. H. & Wilkens, M. Electron microscopical contrast of small cavities in metals, in *6th European Congress on Electron Microscopy* p. 538 (Tal International Publishing Company, Jerusalem, 1976).
24. Stobbs, W. M. Electron microscopical techniques for the observation of cavities. *J. Microscopy* **116,** 3–13 (1979).
25. Ono, S., Ichinose, H. & Masuko, N. Lattice images of crystalline anodic alumina formed on a ridged aluminum substrate. *J. Electrochem. Soc.* **139,** L80–L81 (1992).
26. Ono, S., Ichinose, H. & Masuko, N. Defects in porous anodic films formed on high purity aluminum. *J. Electrochem. Soc.* **138,** 3705–3710 (1991).
27. Macdonald, D. D. On the formation of voids in anodic oxide films on aluminum. *J. Electrochem. Soc.* **140,** L27–L30 (1993).
28. Mei, Y. F., Wu, X. L., Shao, X. F., Huang, G. S. & Siu, G. G. Formation mechanism of alumina nanotube arrays. *Phys. Lett. A* **309,** 109–113 (2003).
29. Zhu, X. F., Li, D. D., Song, Y. & Xiao, Y. H. The study of oxygen bubbles of anodic alumina based on high purity aluminum. *Mater. Lett.* **59,** 3160–3163 (2005).
30. Habazaki, H. *et al.* Incorporation of transition metal ions and oxygen generation during anodizing of aluminum alloys. *Corros. Sci.* **46,** 2041–2053 (2004).
31. Garcia-Vergara, S. J., Skeldon, P., Thompson, G. E. & Habazaki, H. A flow model of porous anodic film growth on aluminum. *Electrochim. Acta* **52,** 681–687 (2006).
32. Garcia-Vergara, S. J., Skeldon, P., Thompson, G. E., Hashimoto, T. & Habazaki, H. Compositional evidence for flow in anodic films on aluminum under high electric fields. *J. Electrochem. Soc.* **154,** C540–C545 (2007).
33. Jessensky, O., Müller, F. & Gösele, U. Self-organized formation of hexagonal pore arrays in anodic alumina. *Appl. Phys. Lett.* **72,** 1173–1175 (1998).
34. Parkhutik, V. P. & Shershulsky, V. I. Theoretical modeling of porous oxide growth on aluminum. *J. Phys. D* **25,** 1258–1263 (1992).
35. Güntherschulze, A. & Betz, H. Die Bewegung der Ionengitter von Isolatoren bei extremen elektrischen Feldstärken. *Z. Phys.* **92,** 367–374 (1934).
36. Cabrera, N. & Mott, N. F. Theory of the oxidation of metals. *Rep. Prog. Phys.* **12,** 163–184 (1948).
37. Thompson, G. E. & Wood, G. C. Porous anodic film formation on aluminum. *Nature* **290,** 230–232 (1981).
38. Ono, S. & Masuko, N. The duplex structure of cell walls of porous anodic films formed on aluminum. *Corros. Sci.* **33,** 503–507 (1992).
39. Lee, W., Jin, M.-K., Yoo, W.-C. & Lee, J.-K. Nanostructuring of a polymeric substrate with well-defined nanometer-scale topography and tailored surface wettability. *Langmuir* **20,** 7665–7669 (2004).
40. Li, A.-P., Müller, F., Birner, A., Nielsch, K. & Gösele, U. Fabrication and microstructuring of hexagonally ordered two-dimensional nanopore arrays in anodic alumina. *Adv. Mater.* **11,** 483–487 (1999).
41. Cheng, W., Wang, J., Jonas, U., Fytas, G. & Stefanou, N. Observation and tuning of hypersonic bandgaps in colloidal crystals. *Nature Mater.* **5,** 830–836 (2006).

Acknowledgements

We thank F. Müller for helpful discussions and comments on the manuscript. We also thank S. Hopfe for TEM sample preparation and K. Sklarek for SEM measurements. K.S. thanks the International Max Planck Research School for Science and Technology of Nanostructures for a scholarship. We acknowledge financial support from the German Research Foundation (STE 1127/8-1).
Correspondence and requests for materials should be addressed to W.L.
Supplementary Information accompanies this paper on www.nature.com/naturenanotechnology.